*7944–7953* *Nucleic Acids Research, 2016, Vol. 44, No. 16* *Published online 4 July 2016*
*doi: 10.1093/nar/gkw598*

# Mechanism of endonuclease cleavage by the HigB toxin

**Marc A. Schureck, Adrienne Repack, Stacey J. Miles, Jhomar Marquez and Christine M. Dunham***

Emory University School of Medicine, Department of Biochemistry, 1510 Clifton Road NE, Atlanta, GA 30322, USA

Received March 23, 2016; Revised June 17, 2016; Accepted June 22, 2016



## ABSTRACT

**Bacteria encode multiple type II toxin–antitoxin modules that cleave ribosome-bound mRNAs in response to stress. All ribosome-dependent toxin family members structurally characterized to date adopt similar microbial RNase architectures despite possessing low sequence identities. Therefore, determining which residues are catalytically important in this specialized RNase family has been a challenge in the field. Structural studies of RelE and YoeB toxins bound to the ribosome provided significant insights but biochemical experiments with RelE were required to clearly demonstrate which residues are critical for acid-base catalysis of mRNA cleavage. Here, we solved an X-ray crystal structure of the wild-type, ribosome-dependent toxin HigB bound to the ribosome revealing potential catalytic residues proximal to the mRNA substrate. Using cell-based and biochemical assays, we further determined that HigB residues His54, Asp90, Tyr91 and His92 are critical for activity *in vivo*, while HigB H54A and Y91A variants have the largest effect on mRNA cleavage *in vitro*. Comparison of X-ray crystal structures of two catalytically inactive HigB variants with 70S-HigB bound structures reveal that HigB active site residues undergo conformational rearrangements likely required for recognition of its mRNA substrate. These data support the emerging concept that ribosome-dependent toxins have diverse modes of mRNA recognition.**

## INTRODUCTION

Toxin–antitoxin complexes regulate bacterial physiology in response to changing environmental conditions. These gene pairs are organized into five classes depending on the mode of toxin inhibition by the antitoxin (1). During non-stress conditions, the type II toxin–antitoxin protein–protein complexes are tightly associated and the antitoxin functions as a transcriptional repressor by binding at upstream DNA operator sites to sterically block RNA polymerase access to the promoter region. Different types of stress cause antitoxin degradation, releasing the toxin which, in turn, inhibits essential growth processes including replication, ribosome assembly, protein synthesis and cell wall synthesis or affects mRNA, tRNA and cytoskeletal stability (2–8). As part of the bacterial stress response, type II toxins are beneficial to the bacterial host as these proteins are critical for survival and are therefore not intrinsically 'toxic' (9). For example, type II toxins have recently been shown to promote the transition to an antibiotic-tolerant state known as persistence (9–14). Therefore, understanding the molecular mechanism of action of toxin–antitoxin complexes is critical to exploit the potential of these novel antimicrobial targets.

A majority of type II toxins are RNases that inhibit translation but others include modification enzymes (e.g. HipA or Doc) or proteins that inhibit growth by direct binding of replication machinery such as DNA gyrase (e.g. CcdB) (2,15–17). Toxins predominantly inhibit protein synthesis by cleaving mRNAs in the aminoacyl (A) site of the ribosome (4,18–20), where tRNAs bind to decode mRNA. Other mechanisms by which toxins inhibit translation include cleavage of ribosomal RNA at functionally important sites (21–23), cleavage at the anticodons of tRNAs (5,24) and modification of glutamyl-tRNA synthase (17) or elongation factor Tu (15,16). While initially thought to inhibit protein synthesis during stress to illicit a global response, it may be that toxin activation leads to specific changes in expression required for survival and that each activated toxin is tuned to the particular stress encountered by the bacterium.

X-ray crystal structures of *Escherichia coli* RelE and YoeB, and *Proteus vulgaris* HigB toxins bound to the 70S ribosome revealed a number of potential catalytic residues that surround the mRNA substrate and which may be important for mRNA cleavage activity (18–20). These ribosome-dependent toxins resemble small, microbial RNases like Sa and T1 that have concave active sites where RNA substrates bind (25,26). Ribosome-dependent

*To whom correspondence should be addressed. Tel: +1 404 712 1756; Fax: +1 404 727 2738; Email: christine.m.dunham@emory.edu

toxins also use a similar mechanism of acid-base catalysis to cleave the mRNA phosphodiester backbone (18,19). Such reactions are characterized by deprotonation of the 2′-OH of the nucleotide preceding the scissile phosphate (27). This deprotonation promotes attack by the 2′ oxygen at the scissile phosphate forming a trigonal bipyramidal intermediate with the accumulating negative charge on the 5′ oxyanion leaving group stabilized by the donation of proton. Despite the significant insights provided by structures of toxins bound to the ribosome, which toxin residues play active and essential roles in catalysis remains unclear. One reason for this ambiguity is the low sequence identity among active site residues of ribosome-dependent toxins and with their homologs RNase Sa and T1. Another confounding factor is the large number of toxin residues that are proximal to the active site that could potentially participate in mRNA cleavage. For example, although RelE residue Tyr87 is the closest residue to the 2′-OH of the mRNA substrate (∼3.8 Å), suggesting a role as the general base (18), more recent kinetic analyses revealed that instead RelE residue Lys52 or Lys54 is the general base (28,29). RelE Arg81 is adjacent to the 5′-oxyanion leaving group and likely donates a proton during the reaction (28–30). Since ribosome-dependent toxins YoeB, YafQ and HigB lack analogous lysine or arginine residues to those found in RelE, this suggests that alternative mechanisms of mRNA substrate recognition and cleavage may exist for different bacterial toxins.

The *P. vulgaris* ribosome-dependent toxin HigB preferentially cleaves at adenosine-rich codons (31). The requirement for a single adenosine in the three-nucleotide codon suggested a different mode of mRNA recognition on the ribosome compared to how tRNAs decode mRNA. To understand how HigB recognizes mRNA, we previously reported X-ray crystal structures of a catalytically inactive HigB bound to both the AAA and ACA codons in the A site of the 70S (20). These studies showed that upon HigB binding to the ribosome, HigB residues and 16S rRNA nucleotides form an adenosine-specific pocket around the third nucleotide of the codon, providing a rationale for the preference of an adenosine nucleotide at this position. Additionally, we determined that HigB residue Asn71, which forms an integral part of the pocket surrounding the third adenosine of the codon, is critical for this adenosine specificity. These data began to provide a mechanistic framework for how ribosome-dependent toxins like HigB recognize and cleave mRNA transcripts in response to stress.

To trap precleavage state structures on the ribosome in previous structures, we used a catalytically inactive HigB variant that is deficient in mRNA cleavage but which still associates with the ribosome (31) in combination with mRNA modified to also prevent cleavage (20). A number of HigB active site residues that could potentially function in acid-base catalysis were identified but their roles were not directly tested. We also wondered if the use of the HigB catalytic variant compromised its active site architecture and, thus, obscured the identification of HigB residues critical for activity. Therefore, to reconcile this possible discrepancy, we report here the X-ray crystal structure of wild-type HigB bound to the 70S containing an A-site AAA lysine codon with 2′-O-methyl modifications on each ribose to prevent cleavage. We additionally performed biochemical and cellular assays to comprehensively test which HigB residues are critical for function. Our cell-based and kinetic assays reveal that HigB residues His54, Asp90, Tyr91 and His92 are critical for activity. Furthermore, high resolution X-ray crystal structures of HigB variants that have defects in catalysis provide insights into the organization of the active site residues before and after recognition of ribosome-bound mRNA.

## MATERIALS AND METHODS

### Strains and plasmids

*E. coli* BW25113 cells [Δ(*araD-araB*)*567* Δ(*rhaD-rhaB*)*568 ΔlacZ4787* (::rrnB-3) *hsdR514 rph-1*] (32) were transformed with pBAD24-HigB, pBAD-Myc-HisA-HigB(His)$_6$ or HigB mutants plasmids, kind gifts from Prof. Nancy A. Woychik (Rutgers University). HigB mutations were introduced by site-directed mutagenesis followed by DNA sequencing (Genewiz) (Supplementary Table S1).

### Wild-type HigB and HigB variant expression and purification

HigB and HigB variants were overexpressed and purified essentially as wild-type HigB (20) with the exception that $Ni^{2+}$ affinity purification of the HigB variants was manually performed with $Ni^{2+}$ Sepharose High Performance Resin (GE Healthcare). BW25113 cells transformed with the pBAD-Myc-HisA-HigB(His)$_6$ wild-type or HigB variants were grown at 37°C overnight in M9 minimal medium (48 mM $Na_2HPO_4$, 22 mM $KH_2PO4$, 8.6 mM $NH_4Cl$, 18.7 mM NaCl, 1 mM $MgSO_4$, 0.1 mM $CaCl_2$ and 0.2% (w/v) casamino acids) supplemented with 0.2% (w/v) glucose to minimize leaky expression. An expression culture was inoculated (1:100) and grown at 37°C in minimal medium supplemented with 0.21% (w/v) glycerol. Protein expression was induced with 0.04% (w/v) arabinose at an optical density of 0.7 at 600 nM. After 3 h, cultures were pelleted by centrifugation and pellets were frozen at −20°C. Cells were disrupted by sonication and debris was separated by centrifugation. Cell lysate was applied to $Ni^{2+}$ Sepharose resin (GE Healthcare) and fractions containing HigB were further purified on a S75 10/300 size exclusion column (GE Healthcare). For the 70S crystal structure and mRNA cleavage assays, the hexa-histidine tag was not removed. For the crystallization of the free HigB protein, the hexa-histidine tag and a portion of the linker were removed by trypsin proteolysis prior to crystallization leaving seven C-terminal linker residues.

### 70S purification, complex formation and 70S-HigB structure determination

*Thermus thermophilus* 70S ribosomes were purified and crystallized as previously described (20,33). 70S ribosomes were incubated with CC-Puromycin to bind at the 50S A site, mRNA (IDT; 5′-GGCAAGGAGGUAAAAAUGAmAmAmUAGU-3′, where the 'm' indicates A-site 2′-O methyl modifications to prevent mRNA cleavage) and P-site $tRNA^{fMet}$ (Chemical Block). Crystals grew to dimensions of 70 × 70 × 400 μM in one week in a final concentration of 0.1 M Tris-HCl,

pH 7.0, 0.2 M KSCN, 3.75–4.5% PEG 20K and 3.75–4.5% PEG 550 MME. Both PEG concentrations were raised to 7% (w/v) and crystals were incubated with HigB (100 μM) for 1.5 h. Crystals were cryoprotected in a step-wise manner to a final concentration of 30% PEG 550 MME before plunging in liquid nitrogen. X-ray diffraction data were collected at the Northeast Collaborative Access Team (NE-CAT) ID24-C beamline at the Advanced Photon Source (Argonne, IL, USA) and processed with the XDS software (34) (Supplementary Table S2). The structure was solved using a 70S-HigB ΔH92 precleavage state model lacking HigB and A-site mRNA as a start model (PDB code 4YZV) (20). HigB residues 1–90 were placed into unbiased electron difference density and manual model building was performed in Coot (35) followed by iterative rounds of refinement in PHENIX (36). mRNA was visible for the E-site, P-site and A-site codons and one nucleotide 3′ of the A-site AAA codon. The positions of 16S rRNA, 23S rRNA, mRNA and tRNAs were refined using the individual site refinement procedure with base-pair restraints in PHENIX, while HigB was refined individually with secondary structure restraints.

### Bacterial growth or toxicity assays

Bacterial growth assays were performed in *E. coli* BW25113 as previously described (31). Wild-type HigB and HigB variants were expressed from the pBAD24-HigB plasmid by induction with 0.2% arabinose and bacterial growth monitored every hour for 6 h after induction. In this assay, growth indicates that the corresponding amino acid substitution has inactivated HigB. The average $OD_{600}$ values and associated standard error of the mean (SEM) were plotted in GraphPad Prism 5. For HigB variants that had robust growth, we performed Western blot analysis to confirm the presence of soluble HigB protein as previously described (31).

### Single-turnover kinetic measurements

*E. coli* 70S ribosomes were purified as previously described (37). 70S (1.2 μM) were programmed with 5′-$^{32}$P-labeled mRNA (0.6 μM; 5′-GGC*AAGGAG*GUAAAA<u>AUG</u>AAAUAGU-3-′ (IDT; Shine-Dalgarno sequence is italicized and the AUG start codon is underlined)) for 6 min at 37°C to ensure all mRNA was ribosome bound. *E. coli* $tRNA^{fMet}$ (3 μM; Chemical Block) was next incubated for 30 min to allow for binding at the P site. Wild-type or variant HigB (10 μM) was added to the 70S mixture and incubated at 37°C for 120 min. Aliquots were taken at 0.5 (wild-type only), 1, 3, 10, 30, 60 and 120 min, diluted 2-fold in formamide dye, heated to 70°C for 2 min to halt the reaction and stored on ice or at −20°C. Samples were analyzed on a preheated, 8 M urea, 1X TBE, 18% polyacrylamide sequencing gel for 1 h and the gel was fixed, dried and exposed to a phosphor storage screen. The intensities of the $^{32}$P-labeled mRNA were measured by Typhoon FLA 7000 (GE Healthcare) and quantified by the program Image Quant. The pmols of mRNA cleaved was calculated for each time point using the following formula: 12 pmol × (intensity of cleaved band)/(intensity of cleaved band + intensity of uncleaved band). The product progression curves were fit by non-linear regression using the software GraphPad PRISM 5 (GraphPad Software Inc.): [Product] = $P_{max}$ (1 $-e^{-kt}$), where $P_{max}$ is the product plateau level, $k$ is the observed rate constant and t is the reaction time (Table S3). For wild-type HigB and HigB R73A, the calculated plateau was unrestrained and yielded ∼11 pmol cleaved. For the remainder of the HigB variants, which did not reach 11 pmol cleaved, the maximum plateau was restrained to 11 pmol.

### Structure determination of *P. vulgaris* HigB variants

Crystals of trypsinized HigB Y91A and HigB ΔH92 were grown in the same condition as wild-type HigB (30-40% w/v PEG 2000 MME and 0.15 M KBr) (20). Crystals were cryoprotected in a stepwise manner to a final cryoprotectant solution of 10% w/v PEG 2000 MME and 30% v/v ethylene glycol. X-ray crystallography data sets were collected at the Southeast Regional Collaborative Access Team (SER-CAT) 22-ID beamline at the APS. X-ray data were processed with the XDS software (34) (Y91A) or HKL2000 (38) (ΔH92) (Supplementary Table S4). All structures were solved by molecular replacement using a polyalanine model of HigB (PDB code 4PX8) in the AutoMR program in PHENIX (36). Although all HigB variants crystallized in the C2 spacegroup, HigB Y91A crystallized with eight copies per asymmetric unit while the HigB ΔHis92 asymmetric unit only contained one HigB molecule. An initial round of automated model building was performed in PHENIX with the autobuild program, followed by iterative rounds of manual model building in Coot (35) and refinement in PHENIX (36). The x,y,z coordinates, occupancies and anisotropic B-factors were refined. For the HigB Y91A structure at 1.55 Å, water B-factors were refined isotropically. In both the HigB Y91A and HigB ΔH92 structures, all HigB residues were built (1–92 and 1–91, respectively) along with the seven C-terminal linker residues that remained after proteolysis.

## RESULTS

### Structure determination of the 70S - wild-type HigB complex

We previously solved three X-ray crystal structures of the *Thermus thermophilus* 70S bound to the HigB toxin in both a precleavage or a postcleavage state (20). The precleavage states contained a HigB variant lacking His92 (ΔH92) bound to A-site AAA lysine and ACA threonine codons modified with a 2′-O methyl modification to prevent cleavage (20). We selected this HigB variant because previous studies demonstrated the importance of His92 whereby the H92Q substitution inactivated HigB function yet still allowed for association with ribosomes (31). This structure provided significant insights into how HigB interacts with the mRNA substrate in the A site and which HigB residues may be catalytic. However, as His92 is clearly important for mRNA cleavage, the deletion of His92 may inactivate HigB by interfering with active site organization thus making the identification of potentially critical residues difficult.

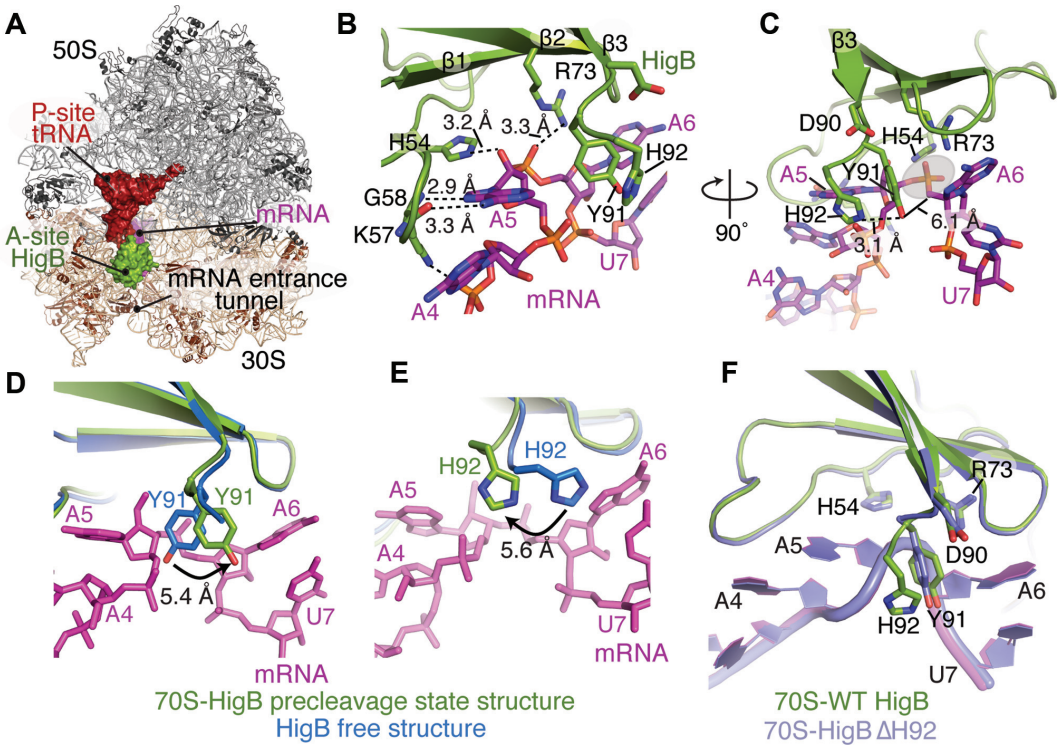


**Figure 1.** Recognition of the ribosomal A site by endonuclease HigB. (**A**) 3.6-Å X-ray crystal structure of HigB bound to a AAA lysine codon containing 2′-O-methyl modifications to prevent cleavage. The side view shows the A site in the forefront with the P-site tRNA (red) behind. (**B**) A 90° rotation of (A) and zoomed view reveals how HigB engages the AAA mRNA substrate. The mRNA is numbered from the P-site AUG codon (starting with +1) with A4, A5 and A6 nucleotides residing in the A site. The panel emphasizes how HigB residues K57 and H54 form hydrogen bonding interactions with the A5 nucleotide, with HigB residue R73 interacting with the scissile phosphate. (**C**) A 90° rotation of (B) to highlight that Y91 is the closest residue to the 5′ leaving group (6.1 Å; shaded circle) with H92 proximal to Y91 (3.1 Å). (**D**) Alignment of the free HigB structure (PDB code 4PX8; blue) to 70S- wild-type HigB (this study; green) in a precleavage state structure (AmAmAm codon; magenta). HigB residue Y91 reorganizes to prevent clashing with the scissile phosphate when recognizing the ribosomal A site. (**E**) The same comparison as in (D) except focuses on HigB residue H92 that repositions upon binding to the ribosomal A site to avoid a steric clash with the nucleobase of A6. (**F**) Comparison of 70S-wild-type HigB (this study) and 70S-HigB ΔHis92 (PDB code 4YPB) both in precleavage states. These structures were least-square fit aligned in Coot (35) using the body domain of the 30S subunit (16S rRNA residues 560–912). For the 70S- wild-type HigB precleavage structure, HigB is depicted in green, mRNA in magenta and 16S rRNA in tan. All components of the 70S-HigB ΔHis92 structure are shown in light purple.

To gain further insight into the mechanism of mRNA cleavage by HigB, here we solved the X-ray crystal structure of wild-type HigB bound to the 70S with a preferred AAA codon in the A site (Figure 1; Supplementary Table S2). The complex was trapped in the precleavage state by including 2′-O methyl modifications at all three A-site nucleotides. The 70S-HigB structure was determined to 3.6 Å ($I/\sigma$ = 1.8) and clear $F_o$–$F_c$ difference electron density maps allowed unambiguous placement of P-site $tRNA^{fMet}$, mRNA and A-site bound HigB (Supplementary Figure S1).

HigB is a small globular protein (10.7 kDa) that adopts a microbial ribonuclease fold similar to RNases Sa, U2 and T1 and contains a distinctive cleft of active site residues that interacts with the A-site mRNA substrate (Figure 1B and C) (39–41). HigB is a member of the RelE/YoeB family of bacterial toxins that also includes *E. coli* YafQ (42–46). The tertiary fold of this family is characterized by a single β-sheet surrounded by 2–4 surface-exposed, α-helices that mediate interactions with the negatively charged 16S rRNA backbone. Upon binding the ribosomal A site, HigB pulls the mRNA ∼9 Å from the normal mRNA path into its concave active site to interact with each of the three nucleotides of the mRNA codon in distinct ways (20). This displacement also causes the mRNA to adopt a distorted conformation likely required to properly orient the mRNA substrate for in-line or $S_N2$ attack at the scissile phosphate that is located between the second and third A-site nucleotides. Adjacent to the peptidyl (P) site, the first adenosine of the A-site codon (A4, where the mRNA numbering begins with the P-site AUG start codon as +1, +2 and +3) is sandwiched between HigB residue Lys57 and the P-site $tRNA^{fMet}$ but its nucleobase makes no direct hydrogen bonding or electrostatic interactions with HigB. HigB more closely monitors the second A-site adenosine (A5) by forming hydrogen bonds with the backbone carbonyl and amino groups of HigB residue Lys57 with the A5 Hoogsteen face while the side chain of His54 forms a hydrogen bond with the 2′-OH of A5 (Figure 1B). The scissile phosphate is contacted by Arg73 and the closest residue to the 5′-oxyanion leaving group is Tyr91 (Figure 1C). Although His92 was shown to be important for function (47), it is adjacent to Tyr91. The third A-site adenosine is splayed from its normal position allowing its Hoogsteen face to hydrogen bond with the Watson–Crick face of 16S rRNA nucleotide C1054. This structure provides insights into potential catalytic HigB residues.

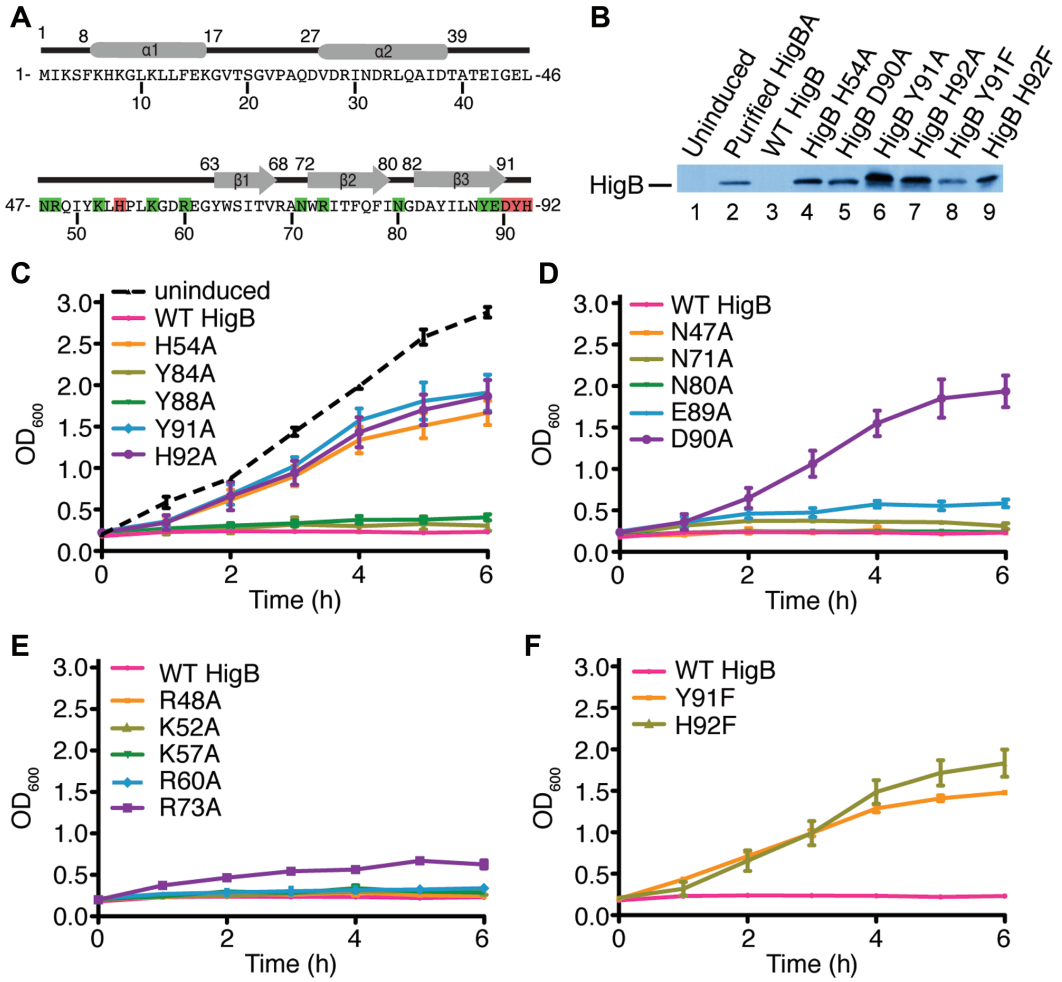


**Figure 2.** Identification of essential HigB residues. (**A**) *P. vulgaris* HigB sequence labeled with its secondary structure. Residues essential for function in bacterial growth assays are highlighted in red and non-essential residues highlighted in green. (**B**) Western blot analysis of the soluble fraction from the bacterial growth assays that permit growth (panels C–F) at 4 h postinduction using polyclonal antibodies against the HigBA toxin–antitoxin complex. Overexpression of wild-type HigB results in an inhibition of protein synthesis with no detectable HigB protein in the immunoblot (lane 3). (**C**) Bacterial growth assays where wild-type HigB and HigB variants are overexpressed. HigB residues that cluster around the mRNA were substituted with alanine and their effect on *E. coli* growth was monitored at 600 nm for 6 h after protein induction. HigB aromatic residues proximal to the scissile phosphate were changed to alanine. Uninduced HigB H54A is shown in the black dotted line. HigB charged and acidic residues proximal to the (**D**) HigB active site and (**E**) HigB basic residues that interact with or are proximal to the mRNA phosphate backbone were substituted with alanine and their effect on bacterial growth was monitored. (**F**) HigB aromatic residues whose functional side chains were mutated to neutral phenylalanine to retain its aromatic stacking ability. Error bars display standard error of the mean from at least three experiments.

Previously, we solved a high-resolution X-ray structure of the wild-type HigB toxin and upon comparison with the 70S-HigB structure (this study), HigB active residues Tyr91 and His92 both undergo ∼5 Å movements upon binding mRNA on the ribosome (Figure 1D and E). This movement appears critical as the side chains of Tyr91 and His92 of the free HigB would sterically clash with the scissile phosphate and nucleobase of A6, respectively. In the context of the 70S-wild-type HigB complex structure, the side chain hydroxyl group of Tyr91 is located ∼6.1 Å from the 5′ oxygen leaving group of A6. The side chain amine group of His92 is located ∼3.1 Å from the hydroxyl side chain of Tyr91 forming a hydrogen bonding network.

### Effect of HigB variants on growth suppression

To understand which HigB residues are important for function, we generated HigB variants of proposed active site residues and tested their function in bacterial growth assays (Figure 2A). Overexpression of wild-type HigB halts bacterial growth (31,48). Therefore, in this assay, upon specific amino acid substitution, restoration of growth is interpreted as the loss of HigB activity, implicating the residue as essential for HigB function. Aromatic HigB residues Tyr84 and Tyr88 are proximal to the HigB active site but substitution of either residue to alanine has no effect on growth suppression as compared to wild-type HigB suggesting these residues are not critical for mRNA cleavage (Figure 2C). Polar and acidic HigB residues Asn47, Asn71, Asn80 and Glu89 may influence the pKa of active site residues similar

to the role proposed for Asp61 or Asp67 in YafQ (37). Our bacterial growth assays reveal no change on HigB-mediated growth suppression upon substitution to alanine for any of these residues (Figure 2D). RelE toxin mediates mRNA cleavage using two basic residues (either Lys52 or Lys54, and Arg81) (28,29). We therefore made substitutions of a number of basic HigB residues close to the mRNA path including Arg48, Lys52, Lys57, Arg60 and Arg73 but again, we found that no single residue was essential, although the HigB R73A variant had a modest impact on HigB toxicity (Figure 2E). HigB residue His54 is close to the 2′-OH of nucleotide A5, the position that becomes deprotonated to initiate the reaction, while Asp90, Tyr91 or His92 are adjacent to the scissile phosphate (Figure 1B). Cell growth is completely restored when HigB residues His54, Asp90, Tyr91 or His92 are mutated to alanine demonstrating their functional importance (Figure 2C, D and E). To determine if either Tyr91 or His92 is critical for structurally orienting the mRNA substrate or if either directly participates in mRNA catalysis, we changed each to phenylalanine and observed the impact on bacterial growth. Substitution of HigB residue His92 with phenylalanine removes the ability of the histidine side chain amide to interact with the hydroxyl of Tyr91 but would allow preservation of interactions such as stacking between the two aromatic residues (Figure 1C). In the case of HigB residue Tyr91 substitution with phenylalanine, the variant would be solely deficient in catalysis due to the loss of the hydroxyl side chain which is located ∼6 Å from the 5′ leaving group of the mRNA substrate. In both cases, HigB Y91F and H92F variants reverse the HigB toxicity and allow for normal bacterial growth (Figure 2F). These results strongly suggest that residues Tyr91 and His92 play critical roles in mRNA cleavage rather than contributing to base stacking. Consistent with what we observe in the growth assays, all HigB variants that restore growth are expressed and soluble, and therefore, the reversal in the growth phenotype can be attributed to disruption of HigB function (Figure 2B).

Collectively, these assays identified four HigB residues (His54, Asp90, Tyr91 and His92) as important for activity *in vivo*. Moreover, these results suggest that basic residues are not critical for HigB-mediated mRNA cleavage, in contrast to RelE (28,29). Instead, HigB functions more similarly to ribosome-dependent toxins that utilize histidine and glutamate residues (YoeB, Glu46 and His83; YafQ, His50 and His87) (19,37).

### HigB residues His54, Asp90, Tyr91 and His92 are critical for mRNA cleavage

To determine whether each of the four HigB residues identified in the growth assays directly affects mRNA cleavage, we performed *in vitro* single turnover mRNA cleavage assays. We incubated 5′-$^{32}$P-labeled mRNA containing a Shine–Dalgarno upstream of an AUG start codon positioned in the P site and an AAA lysine codon in the A site with a two-molar excess of *E. coli* 70S. We next programmed with tRNA$^{fMet}$ in the P site and added a saturating 17-fold molar excess of wild-type HigB and monitored mRNA cleavage over 120 min (Figure 3A and B; Supplementary Figure S2 and Supplementary Table S3). The YafQ toxin binds to an identical *E. coli* 70S programmed complex with an affinity (∼360 nM) that is within the same order of magnitude as A-site binding tRNAs (20–500 nM) and initiation factors 1 and 3 (600 and 440 nM, respectively) (37,49,50). In this assay, the concentration of HigB (10 μM) is well above its predicted binding constant to the 70S ribosome. Therefore, the results from this assay are likely informing on the catalysis of the reaction and not on the differences in binding of the different HigB variants, but this possibility cannot be excluded. Wild-type HigB cleaved mRNA with a rate constant of 0.46 ± 0.026 min$^{-1}$ whereas HigB variants showed between 11- to 215-fold reductions in mRNA cleavage. Consistent with not fully ablating HigB toxicity *in vivo*, HigB R73A shows an 11-fold reduction in the rate constant of mRNA cleavage and the H54A variant exhibits a 52-fold reduction in the cleavage rate. HigB C-terminal residues Asp90, Tyr91 and His92 are highly conserved among HigB homologs and their substitutions with alanine caused the largest effect on the mRNA cleavage rate constants. HigB variants D90A, Y91A, H92A and ΔHis92 reduced the cleavage rate constant by 77-, 215-, 184- and 190-fold, respectively. These data confirm that HigB residues His54, Asp90, Tyr91 and His92 are critical for mRNA cleavage.

### Structures of free HigB Y91A and HigB ΔH92

To understand the impact these variants have on the integrity of the HigB active site, we next solved X-ray crystal structures of the HigB variants Y91A and ΔHis92 to 1.55 Å and 1.1 Å, respectively (Supplementary Figure S3; Supplementary Table S4). We attempted to solve structure of HigB H54A and H92A variants but were unable to grow diffracting crystals. Comparison of the HigB Y91A and ΔHis92 structures with the wild-type HigB structure (20) (PDB code 4PX8) reveals a similar Cα backbone trace (root mean square deviations (rmsd) = 0.28 and 0.41 Å, respectively) and the only structural changes are located in the active site.

Both Tyr91 and His92 undergo large conformational changes of 5.4 Å and 5.6 Å, respectively, upon binding mRNA on the ribosome (Figure 1D and E). These conformational changes are required otherwise both HigB residues would clash with the mRNA substrate. Our biochemical assays argue that both residues play a role in catalysis as mutation to alanine renders HigB inactive (Figures 2C and 3). However, one other reason could be that the substitution interferes with the optimal rearrangement required for mRNA recognition. Our structure of HigB Y91A reveals that the active site residues His54, Arg73, Asp90 and His92 are minimally perturbed as compared to free, wild-type HigB (Supplementary Figure S3B) suggesting that the substitution likely mainly impacts catalysis. In contrast, the 1.1-Å structure of the HigB ΔHis92 reveals a dramatic reorganization of the active site residues (Supplementary Figure S3C). Arg73 and Tyr91 move ∼6 and 9 Å changes, respectively while Asp90 and Tyr91 exist in alternative conformations. The deletion of His92 causes the backbone and sidechain of Tyr91 to rotate ∼65° away from His54 while the sidechain of Arg73 is shifted ∼180° toward the new position of Tyr91 (Supplementary Figure S3C, bottom). One

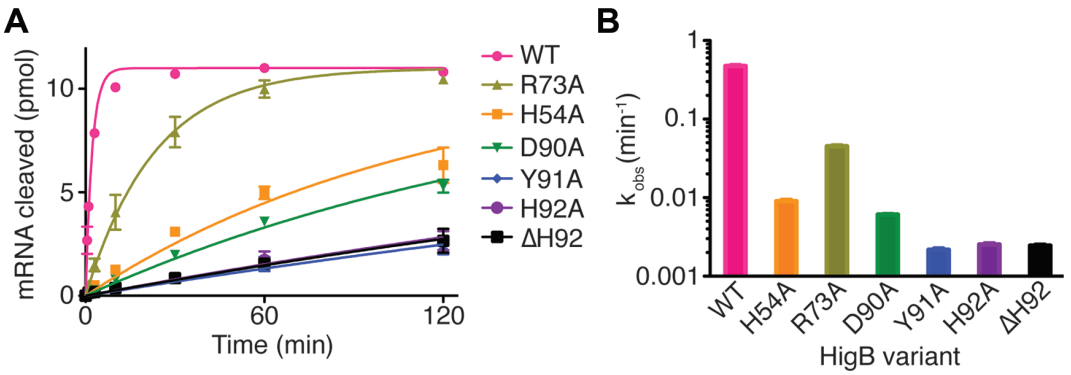


**Figure 3.** Analysis of HigB residues important for mRNA cleavage. (**A**) Product progression curves of wild-type HigB and HigB variants incubated with programmed *E. coli* 70S-mRNA complexes and the amount of mRNA cleaved was monitored under single-turnover conditions. (**B**) $k_{obs}$ values for wild-type HigB and HigB variants derived from panel A. In both panels, error bars display standard deviations from two replicates.

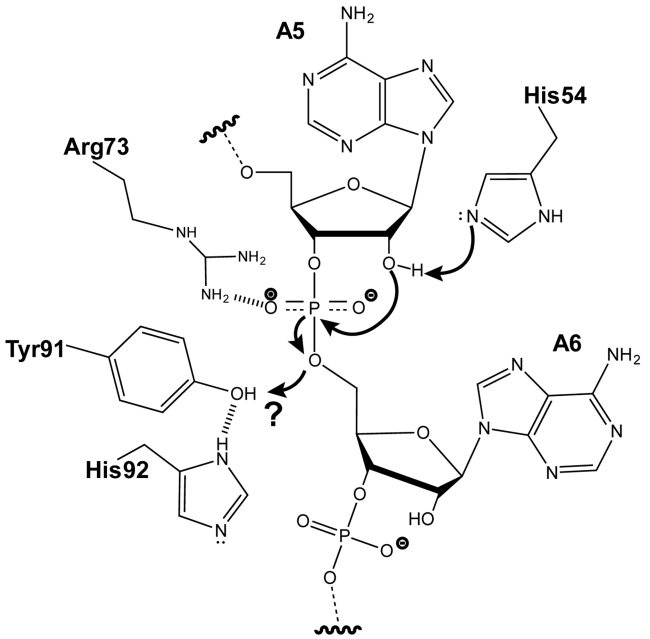


**Figure 4.** Proposed mechanism of HigB-mediated mRNA degradation on the ribosome. View of the HigB active site with proposed catalytic residues His54, Arg73, Asp90, Tyr91 and His92 shown surrounding the mRNA substrate. His54 likely functions as a general base to deprotonate the 2′-proton of the 2′-OH of the A5 nucleotide of the mRNA, Arg73 stabilizes the bipyramidal transition state and Tyr91 possibly stabilizes the 5′- leaving group as a general acid while simultaneously interacting with His92. Both Asp90 and His92 (not shown) may play structural roles to properly orient Tyr91 to donate a proton or may aid by donating a proton to the Tyr91 oxyanion form.

possibility for this dramatic movement could be the result of the deletion, however, in all cases, there are an additional seven C-terminal residues resulting from proteolytic cleavage of the hexa-histidine purification tag (20). Therefore, instead of a true truncation, this HigB variant contains a lysine residue at position 92. His92 in the wild-type HigB structure is adjacent to Asn71 and Asp90 however in the HigB ΔH92 structure, the side chain of 'Lys92' does not interact with Asn71 or Asp90 and instead extends into a solvent channel. We propose that by removing His92 and thus changing the location of residue 92, the C-terminus of HigB is reorganized which in turn, impacts the orientation of Tyr91.

## DISCUSSION

The structure of the HigB toxin in a precleavage state bound to the 70S provided significant insights into the possible catalytic roles of residues surrounding the scissile phosphate of the mRNA (20). However, because a HigB variant was used to trap the toxin on the ribosome, it was unclear if the substitution alters the positions of HigB active site residues. Here, we solved an X-ray crystal structure of wild-type HigB bound to the 70S in a precleavage state trapped by mRNA modifications that prevent cleavage. Our structure reveals that HigB residue His54 is within hydrogen bonding distance of the 2′-OH of the second nucleotide of the A-site codon; Arg73 forms a hydrogen bond with the scissile phosphate before and after mRNA cleavage (20); and Tyr91 is the closest residue to the 5′-oxygen of the leaving group at the third A-site nucleotide and is potentially supported in a catalytic role by the proximal Asp90 and His92 residues (20). Based on structural studies, bacterial growth and single turnover kinetic assays presented in this study, we propose that His54 initiates deprotonation of the 2′-OH of A5, a step required for attack at the scissile phosphate (Figure 4). The basic nature of Arg73 likely helps stabilize the negative charge of the transition state, an important but clearly not critical role in catalysis. Although aromatic residues such as Tyr87 in RelE and Phe91 in YafQ stack with the mRNA nucleobase of A5 to optimally position the substrate (30,37), when we substitute Tyr91 with phenylalanine, HigB is no longer active in our growth assays suggesting stacking is not its primary role (Figure 2F). Based upon these studies, Tyr91 may play a more direct catalytic role in HigB-mediated cleavage. The pKa of tyrosine is typically >>7 and therefore to function as a proton donor in a neutral pH environment, the pKa would need to be perturbed. One possibility is that the local microenvironment of the HigB active site alters the pKa of Tyr91 making this residue more suitable as a proton donor. Precedence for this includes the protein Ketosteroid Isomerase where the pKa of its active site tyrosine is perturbed to 6.3 (51,52).

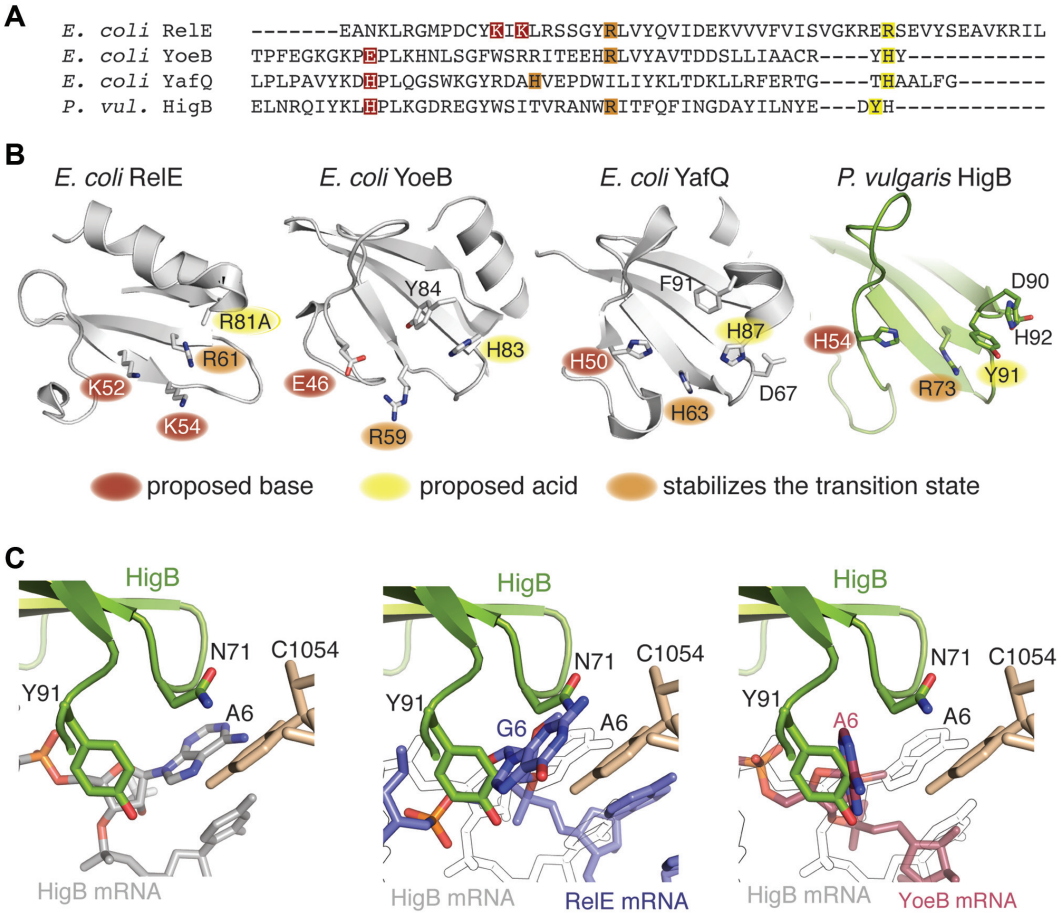


**Figure 5.** Mechanistic differences in how ribosome-dependent toxins recognize the A-site mRNA substrate. (**A**) Sequence alignments of ribosome-dependent toxins RelE, YoeB, YafQ and HigB with the proposed roles of the active site residues highlighted as indicated in panel B. (**B**) Comparisons of ribosome-dependent active site residues (shown as sticks) and their proposed roles in acid-base catalysis (PDB codes 4V7J (70S-RelE), 4V8X (70S-YoeB), 4ML2 (YafQ), 4ZSN (HigB; this study)). (**C**) HigB residues N71 and Y91 flank the A6 A-site nucleotide positioning A6 to interact directly with 16S rRNA residue C1054 (left). Superpositioning of the mRNA upon RelE interaction on the 70S (purple; middle; PDB code 4V7J) and the mRNA upon YoeB interaction on the 70S (pink; right; PDB code 4V8X) reveals significant clashing of HigB residues N71 and Y91 with G6 (middle; mRNA from the 70S-RelE structure) and A6 (right; mRNA from the 70S-YoeB structure). In the middle and right panels, the path of the mRNA when HigB binds the 70S is shown in white with gray outline.

Another consideration is that the pKa of the 5′ oxyanion leaving group is likely much higher than the tyrosine side chain (~13 as compared to ~11). The accumulating negative charge on the 5′ oxyanion could be satisfied by donation of the proton from a tyrosine in this case. However, additional biochemical studies are required to fully answer this question. Based on the impact of similar substitutions of HigB residues Asp90 and His92, we propose these residues likely serve supporting roles in promoting the correct orientation of Tyr91 and/or participation in catalysis through donation of a proton to Tyr91.

Ribosome-dependent toxins only cleave mRNA positioned in the ribosomal A site representing a novel mechanism to regulate translation in response to diverse environmental stress (1,53,54). These toxins facilitate mRNA cleavage at the phosphodiester backbone using acid-base catalysis to leave a 2′-3′ cyclic phosphate (30,37) or a 3′-phosphate product (19). Bacterial genomes contain multiple toxin–antitoxin genes but identifying new toxin–antitoxin modules is one of the challenges in the field because of their low sequence identities even among proposed active site residues (Figure 5A). Although these toxins adopt a microbial RNase fold, each is appended with a diverse set of active site residues. RelE lacks a histidine and charged residue pair typical of canonical RNases (55) and instead, contains basic residues that interact directly with the mRNA substrate and are important for catalysis (Figure 5B) (28–30). In contrast, YoeB contains a histidine-glutamate pair (45), YafQ contains a histidine–histidine pair (37) and HigB uses a histidine–tyrosine pair for catalysis (Figure 5B). These data suggest that RelE is the outlier of ribosome-dependent toxins and the significance of this is unknown.

Although ribosome-dependent toxins contain diverse active site residues, structures of toxins bound to the 70S in combination with steady-state kinetic analyses are beginning to define both some emerging common themes and specific mechanistic differences (20,28–30,37). RelE, HigB and YoeB all form a selective pocket around the splayed third A-site nucleotide of the mRNA, however, contributions from the ribosome are different (19,20,30) (Figure

5C). For example, RelE and HigB form this pocket with help from 16S rRNA nucleotide C1054 while YoeB residues alone forms the nucleotide-binding pocket (19,20,30). HigB binding to the A site flips the third nucleotide from the mRNA path that positions its Hoogsteen edge to interact directly with the Watson–Crick face of 16S rRNA nucleotide C1054 likely contributing significantly to the selection of an adenosine at this third A-site position (Figure 5C). Superpositioning of RelE- or YoeB-bound mRNA in place of the HigB-bound mRNA reveals that HigB active site residues Asn71 and Tyr91 would significantly clash with either G6 (RelE) or A6 (YoeB) nucleotides located in the selective pocket (Figure 5C). These data suggest that although the local position of the general acid for each ribosome-dependent toxin (RelE Arg81, YoeB His83 and YafQ His87) is similar (Figure 5B), each toxin has a different residue that donates a proton to the 5′ oxyanion leaving group that, in turn, engages the nucleotide at the +6 position in different manners. Thus, the general acid and recognition of the third A-site nucleotide appear to be coupled. In summary, these studies contribute to our understanding of the rules that govern toxin selectivity for different mRNA transcripts however, the biological consequence for this exquisite mRNA specificity during bacterial stress still remains an open question.

## ACCESSION NUMBERS

Data deposition: Crystallography, atomic coordinates and structure factors have been deposited in the Protein Data Bank, www.pdb.org (PDB codes 4ZSN, 5IWH and 5IXL).

## SUPPLEMENTARY DATA

Supplementary Data are available at NAR Online.

## ACKNOWLEDGEMENT

The authors thank F. M. Murphy IV and staff members of the NE-CAT beamlines for assistance during data collection and Dr G. L. Conn for critical reading of the manuscript.

## FUNDING

National Science Foundation [CAREER award MCB 0953714 to C.M.D.]; National Institute of Health (NIH) [GM093278 to C.M.D.]; Biochemistry, Cell and Developmental Biology Graduate Training Grant [5T32GM8367 to M.A.S]; F31 Fellowship [GM108351 to M.A.S.]; Pew Biomedical Sciences Program [to C.M.D.]. This work is based upon research conducted at the NE-CAT beamline, which are funded by the National Institute of General Medical Sciences from the NIH [P41 GM103403] and at the SER-CAT beamline. The Pilatus 6M detector on 24-ID-C beam line is funded by a NIH-ORIP HEI grant [S10 RR029205]. This research used resources of the Advanced Photon Source, a U.S. Department of Energy (DOE) Office of Science User Facility operated for the DOE Office of Science by Argonne National Laboratory under Contract No. DE-AC02-06CH11357. Funding for open access charge: National Institute of Health [GM093278].

*Conflict of interest statement.* None declared.

## REFERENCES

1. Maisonneuve,E. and Gerdes,K. (2014) Molecular mechanisms underlying bacterial persisters. *Cell*, **157**, 539–548.
2. Bernard,P. and Couturier,M. (1992) Cell killing by the F plasmid CcdB protein involves poisoning of DNA-topoisomerase II complexes. *J. Mol. Biol.*, **226**, 735–745.
3. Zhang,Y. and Inouye,M. (2011) RatA (YfjG), an Escherichia coli toxin, inhibits 70S ribosome association to block translation initiation. *Mol. Microbiol.*, **79**, 1418–1429.
4. Pedersen,K., Zavialov,A.V., Pavlov,M.Y., Elf,J., Gerdes,K. and Ehrenberg,M. (2003) The bacterial toxin RelE displays codon-specific cleavage of mRNAs in the ribosomal A site. *Cell*, **112**, 131–140.
5. Winther,K.S. and Gerdes,K. (2011) Enteric virulence associated protein VapC inhibits translation by cleavage of initiator tRNA. *Proc. Natl. Acad. Sci. U.S.A.*, **108**, 7403–7407.
6. Ainelo,A., Tamman,H., Leppik,M., Remme,J. and Horak,R. (2016) The toxin GraT inhibits ribosome biogenesis. *Mol. Microbiol.*, **100**, 719–734.
7. Mutschler,H., Gebhardt,M., Shoeman,R.L. and Meinhart,A. (2011) A novel mechanism of programmed cell death in bacteria by toxin-antitoxin systems corrupts peptidoglycan synthesis. *PLoS Biol.*, **9**, e1001033.
8. Tan,Q., Awano,N. and Inouye,M. (2011) YeeV is an Escherichia coli toxin that inhibits cell division by targeting the cytoskeleton proteins, FtsZ and MreB. *Mol. Microbiol.*, **79**, 109–118.
9. Germain,E., Roghanian,M., Gerdes,K. and Maisonneuve,E. (2015) Stochastic induction of persister cells by HipA through (p)ppGpp-mediated activation of mRNA endonucleases. *Proc. Natl. Acad. Sci. U.S.A.*, **112**, 5171–5176.
10. Keren,I., Shah,D., Spoering,A., Kaldalu,N. and Lewis,K. (2004) Specialized persister cells and the mechanism of multidrug tolerance in Escherichia coli. *J. Bacteriol.*, **186**, 8172–8180.
11. Maisonneuve,E., Shakespeare,L.J., Jorgensen,M.G. and Gerdes,K. (2011) Bacterial persistence by RNA endonucleases. *Proc. Natl. Acad. Sci. U.S.A.*, **108**, 13206–13211.
12. Maisonneuve,E., Castro-Camargo,M. and Gerdes,K. (2013) (p)ppGpp controls bacterial persistence by stochastic induction of toxin-antitoxin activity. *Cell*, **154**, 1140–1150.
13. Hu,Y., Kwan,B.W., Osbourne,D.O., Benedik,M.J. and Wood,T.K. (2015) Toxin YafQ increases persister cell formation by reducing indole signalling. *Environ. Microbiol.*, **17**, 1275–1285.
14. Helaine,S., Cheverton,A.M., Watson,K.G., Faure,L.M., Matthews,S.A. and Holden,D.W. (2014) Internalization of Salmonella by macrophages induces formation of nonreplicating persisters. *Science*, **343**, 204–208.
15. Castro-Roa,D., Garcia-Pino,A., De Gieter,S., van Nuland,N.A., Loris,R. and Zenkin,N. (2013) The Fic protein Doc uses an inverted substrate to phosphorylate and inactivate EF-Tu. *Nat. Chem. Biol.*, **9**, 811–817.
16. Cruz,J.W., Rothenbacher,F.P., Maehigashi,T., Lane,W.S., Dunham,C.M. and Woychik,N.A. (2014) Doc toxin is a kinase that inactivates elongation factor Tu. *J. Biol. Chem.*, **289**, 7788–7798.
17. Germain,E., Castro-Roa,D., Zenkin,N. and Gerdes,K. (2013) Molecular mechanism of bacterial persistence by HipA. *Mol. Cell*, **52**, 248–254.
18. Neubauer,C., Gillet,R., Kelley,A.C. and Ramakrishnan,V. (2012) Decoding in the absence of a codon by tmRNA and SmpB in the ribosome. *Science*, **335**, 1366–1369.
19. Feng,S., Chen,Y., Kamada,K., Wang,H., Tang,K., Wang,M. and Gao,Y.G. (2013) YoeB-ribosome structure: a canonical RNase that requires the ribosome for its specific activity. *Nucleic Acids Res.*, **41**, 9549–9556.
20. Schureck,M.A., Dunkle,J.A., Maehigashi,T., Miles,S.J. and Dunham,C.M. (2015) Defining the mRNA recognition signature of a bacterial toxin protein. *Proc. Natl. Acad. Sci. U.S.A.*, **112**, 13862–13867.
21. Winther,K.S., Brodersen,D.E., Brown,A.K. and Gerdes,K. (2013) VapC20 of Mycobacterium tuberculosis cleaves the Sarcin-Ricin loop of 23S rRNA. *Nat. Commun.*, **4**, 2796–2804.
22. Schifano,J.M., Edifor,R., Sharp,J.D., Ouyang,M., Konkimalla,A., Husson,R.N. and Woychik,N.A. (2013) Mycobacterial toxin

MazF-mt6 inhibits translation through cleavage of 23S rRNA at the ribosomal A site. *Proc. Natl. Acad. Sci. U.S.A.*, **110**, 8501–8506.
23. Schifano,J.M., Vvedenskaya,I.O., Knoblauch,J.G., Ouyang,M., Nickels,B.E. and Woychik,N.A. (2014) An RNA-seq method for defining endoribonuclease cleavage specificity identifies dual rRNA substrates for toxin MazF-mt3. *Nat. Commun.*, **5**, 3538–3549.
24. Cruz,J.W., Sharp,J.D., Hoffer,E.D., Maehigashi,T., Vvedenskaya,I.O., Konkimalla,A., Husson,R.N., Nickels,B.E., Dunham,C.M. and Woychik,N.A. (2015) Growth-regulating Mycobacterium tuberculosis VapC-mt4 toxin is an isoacceptor-specific tRNase. *Nat. Commun.*, **6**, 7480–7491.
25. Bauerova-Hlinkova,V., Dvorsky,R., Perecko,D., Povazanec,F. and Sevcik,J. (2009) Structure of RNase Sa2 complexes with mononucleotides–new aspects of catalytic reaction and substrate recognition. *FEBS J.*, **276**, 4156–4168.
26. Langhorst,U., Loris,R., Denisov,V.P., Doumen,J., Roose,P., Maes,D., Halle,B. and Steyaert,J. (1999) Dissection of the structural and functional role of a conserved hydration site in RNase T1. *Protein Sci.*, **8**, 722–730.
27. Cochrane,J.C. and Strobel,S.A. (2008) Catalytic strategies of self-cleaving ribozymes. *Acc. Chem. Res.*, **41**, 1027–1035.
28. Griffin,M.A., Davis,J.H. and Strobel,S.A. (2013) Bacterial toxin RelE: A highly efficient ribonuclease with exquisite substrate specificity using atypical catalytic residues. *Biochemistry*, **52**, 8633–8642.
29. Dunican,B.F., Hiller,D.A. and Strobel,S.A. (2015) Transition state charge stabilization and acid-base catalysis of mRNA cleavage by the endoribonuclease RelE. *Biochemistry*, **54**, 7048–7057.
30. Neubauer,C., Gao,Y.G., Andersen,K.R., Dunham,C.M., Kelley,A.C., Hentschel,J., Gerdes,K., Ramakrishnan,V. and Brodersen,D.E. (2009) The structural basis for mRNA recognition and cleavage by the ribosome-dependent endonuclease RelE. *Cell*, **139**, 1084–1095.
31. Hurley,J.M. and Woychik,N.A. (2009) Bacterial toxin HigB associates with ribosomes and mediates translation-dependent mRNA cleavage at A-rich sites. *J. Biol. Chem.*, **284**, 18605–18613.
32. Datsenko,K.A. and Wanner,B.L. (2000) One-step inactivation of chromosomal genes in Escherichia coli K-12 using PCR products. *Proc. Natl. Acad. Sci. U.S.A.*, **97**, 6640–6645.
33. Selmer,M., Dunham,C.M., Murphy,F.V.T., Weixlbaumer,A., Petry,S., Kelley,A.C., Weir,J.R. and Ramakrishnan,V. (2006) Structure of the 70S ribosome complexed with mRNA and tRNA. *Science*, **313**, 1935–1942.
34. Kabsch,W. (2010) Xds. *Acta Crystallogr. D Biol Crystallogr.*, **66**, 125–132.
35. Emsley,P., Lohkamp,B., Scott,W.G. and Cowtan,K. (2010) Features and development of Coot. *Acta Crystallogr. D Biol Crystallogr.*, **66**, 486–501.
36. Adams,P.D., Afonine,P.V., Bunkoczi,G., Chen,V.B., Davis,I.W., Echols,N., Headd,J.J., Hung,L.W., Kapral,G.J., Grosse-Kunstleve,R.W. *et al.* (2010) PHENIX: a comprehensive Python-based system for macromolecular structure solution. *Acta Crystallogr. D Biol Crystallogr.*, **66**, 213–221.
37. Maehigashi,T., Ruangprasert,A., Miles,S.J. and Dunham,C.M. (2015) Molecular basis of ribosome recognition and mRNA hydrolysis by the E. coli YafQ toxin. *Nucleic Acids Res.*, **43**, 8002–8012.
38. Otwinowski,Z. and Minor,W. (1997) In: Carter,JCW and Sweet,RM (eds). *Methods in Enzymology*. Academic Press, NY, Vol. **276**, pp. 307–326.
39. Sevcik,J., Dodson,E.J. and Dodson,G.G. (1991) Determination and restrained least-squares refinement of the structures of ribonuclease Sa and its complex with 3′-guanylic acid at 1.8 A resolution. *Acta Crystallogr. B*, **47**, 240–253.
40. Heinemann,U. and Saenger,W. (1983) Crystallographic study of mechanism of ribonuclease T1-catalysed specific RNA hydrolysis. *J. Biomol. Struct. Dyn.*, **1**, 523–538.
41. Noguchi,S., Satow,Y., Uchida,T., Sasaki,C. and Matsuzaki,T. (1995) Crystal structure of Ustilago sphaerogena ribonuclease U2 at 1.8 A resolution. *Biochemistry*, **34**, 15583–15591.
42. Li,G.Y., Zhang,Y., Inouye,M. and Ikura,M. (2009) Inhibitory mechanism of Escherichia coli RelE-RelB toxin-antitoxin module involves a helix displacement near an mRNA interferase active site. *J. Biol. Chem.*, **284**, 14628–14636.
43. Ruangprasert,A., Maehigashi,T., Miles,S.J., Giridharan,N., Liu,J.X. and Dunham,C.M. (2014) Mechanisms of toxin inhibition and transcriptional repression by Escherichia coli DinJ-YafQ. *J. Biol. Chem.*, **289**, 20559–20569.
44. Liang,Y., Gao,Z., Wang,F., Zhang,Y., Dong,Y. and Liu,Q. (2014) Structural and functional characterization of Escherichia coli toxin-antitoxin complex DinJ-YafQ. *J. Biol. Chem.*, **289**, 21191–21202.
45. Kamada,K. and Hanaoka,F. (2005) Conformational change in the catalytic site of the ribonuclease YoeB toxin by YefM antitoxin. *Mol. Cell*, **19**, 497–509.
46. Schureck,M.A., Maehigashi,T., Miles,S.J., Marquez,J., Cho,S.E., Erdman,R. and Dunham,C.M. (2014) Structure of the Proteus vulgaris HigB-(HigA)2-HigB toxin-antitoxin complex. *J. Biol. Chem.*, **289**, 1060–1070.
47. Hurley,J.M., Cruz,J.W., Ouyang,M. and Woychik,N.A. (2011) Bacterial toxin RelE mediates frequent codon-independent mRNA cleavage from the 5′ end of coding regions in vivo. *J. Biol. Chem.*, **286**, 14770–14778.
48. Tian,Q.B., Ohnishi,M., Murata,T., Nakayama,K., Terawaki,Y. and Hayashi,T. (2001) Specific protein-DNA and protein-protein interaction in the hig gene system, a plasmid-borne proteic killer gene system of plasmid Rts1. *Plasmid*, **45**, 63–74.
49. Qin,D. and Fredrick,K. (2009) Control of translation initiation involves a factor-induced rearrangement of helix 44 of 16S ribosomal RNA. *Mol. Microbiol.*, **71**, 1239–1249.
50. Tapprich,W.E., Goss,D.J. and Dahlberg,A.E. (1989) Mutation at position 791 in Escherichia coli 16S ribosomal RNA affects processes involved in the initiation of protein synthesis. *Proc. Natl. Acad. Sci. U.S.A.*, **86**, 4927–4931.
51. Fafarman,A.T., Sigala,P.A., Schwans,J.P., Fenn,T.D., Herschlag,D. and Boxer,S.G. (2012) Quantitative, directional measurement of electric field heterogeneity in the active site of ketosteroid isomerase. *Proc. Natl. Acad. Sci. U.S.A.*, **109**, E299–E308.
52. Schwans,J.P., Sunden,F., Gonzalez,A., Tsai,Y. and Herschlag,D. (2013) Uncovering the determinants of a highly perturbed tyrosine pKa in the active site of ketosteroid isomerase. *Biochemistry*, **52**, 7840–7855.
53. Yamaguchi,Y., Park,J.H. and Inouye,M. (2011) Toxin-antitoxin systems in bacteria and archaea. *Annu. Rev. Genet.*, **45**, 61–79.
54. Sofos,N., Xu,K., Dedic,E. and Brodersen,D.E. (2015) Cut to the chase–Regulating translation through RNA cleavage. *Biochimie*, **114**, 10–17.
55. Zegers,I., Haikal,A.F., Palmer,R. and Wyns,L. (1994) Crystal structure of RNase T1 with 3′-guanylic acid and guanosine. *J. Biol. Chem.*, **269**, 127–133.